



HAL
open science

Global trends in carbon sinks and their relationships with CO₂ and temperature

M. Fernández-Martínez, J. Sardans, F. Chevallier, Philippe Ciais, M. Obersteiner, S. Vicca, J. Canadell, A. Bastos, P. Friedlingstein, S. Sitch, et al.

► **To cite this version:**

M. Fernández-Martínez, J. Sardans, F. Chevallier, Philippe Ciais, M. Obersteiner, et al.. Global trends in carbon sinks and their relationships with CO₂ and temperature. *Nature Climate Change*, 2019, 9 (1), pp.73-79. 10.1038/s41558-018-0367-7 . hal-02895281

HAL Id: hal-02895281

<https://hal.science/hal-02895281v1>

Submitted on 22 Jun 2021

HAL is a multi-disciplinary open access archive for the deposit and dissemination of scientific research documents, whether they are published or not. The documents may come from teaching and research institutions in France or abroad, or from public or private research centers.

L'archive ouverte pluridisciplinaire **HAL**, est destinée au dépôt et à la diffusion de documents scientifiques de niveau recherche, publiés ou non, émanant des établissements d'enseignement et de recherche français ou étrangers, des laboratoires publics ou privés.

1 **Global trends in carbon sinks and their relationships with CO₂ and**
2 **temperature**

3 **Authors:** M. Fernández-Martínez^{*1}, J. Sardans^{2,3}, F. Chevallier⁴, P. Ciais⁴, M. Obersteiner⁵, S.
4 Vicca¹, J. G. Canadell⁶, A. Bastos⁴, P. Friedlingstein⁷, S. Sitch⁷, S.L. Piao^{8,9}, I.A. Janssens¹, J.
5 Peñuelas^{2,3}.

6 **Affiliations:**

7 ¹ Centre of Excellence PLECO (Plant and Vegetation Ecology), Department of Biology,
8 University of Antwerp, 2610 Wilrijk, Belgium.

9 ² CSIC, Global Ecology Unit, CREAM-CSIC-UAB, Cerdanyola del Vallès, 08193 Barcelona,
10 Catalonia, Spain

11 ³ CREAM, Cerdanyola del Vallès, 08193 Barcelona, Catalonia, Spain

12 ⁴ Laboratoire des Sciences du Climat et de l'Environnement, CEA CNRS UVSQ, 91191 Gif-sur-
13 Yvette, France

14 ⁵ International Institute for Applied Systems Analysis, Schlossplatz 1, 2361 Laxenburg, Austria

15 ⁶ Global Carbon Project, CSIRO Oceans and Atmosphere, Canberra, ACT 2601, Australia

16 ⁷ College of Engineering, Computing and Mathematics, University of Exeter, Exeter EX4 4QF,
17 UK

18 ⁸Sino-French Institute of Earth System Sciences, College of Urban and Environmental
19 Sciences, Peking University, Beijing 100871, China

20 ⁹ Institute of Tibetan Plateau Research, Chinese Academy of Sciences, Beijing 100085, China

21 *Correspondence to: M. Fernández-Martínez, marcos.fernandez-martinez@uantwerpen.be

22

23

24 Elevated CO₂ increases photosynthesis and, potentially, net ecosystem production
25 (NEP) meaning greater CO₂ uptake. Climate, nutrients, and ecosystem structure,
26 however, influence the effect of increasing CO₂. Here, we analysed global NEP from
27 MACC-II and Jena CarboScope atmospheric-inversions and 10 dynamic global
28 vegetation models (TRENDY), using statistical models to attribute the trends in NEP to
29 its potential drivers: CO₂, climatic variables and land-use change. We find that
30 increasing CO₂ was consistently associated with increased NEP (1995-2014).
31 Conversely, increasing temperatures were negatively associated with NEP. Using the
32 two atmospheric inversions and TRENDY, the estimated global sensitivities for CO₂
33 were 6.0 ± 0.1 , 8.1 ± 0.3 and 3.1 ± 0.1 Pg C per 100 ppm (~ 1 °C increase), and $-0.5 \pm$
34 0.2 , -0.9 ± 0.4 and -1.1 ± 0.1 Pg C °C⁻¹ for temperature. These results indicate a
35 positive CO₂ effect on terrestrial C sinks that is constrained by climate warming.

36

37 In recent decades, terrestrial ecosystems have been absorbing 15–30% of all
38 anthropogenic CO₂ emissions^{1,2}. Direct and indirect anthropogenic impacts on the
39 biosphere, however, can alter terrestrial sinks in the short and long terms^{3–6}. Identifying
40 the factors that affect the capacity of the biosphere to absorb carbon (C) and
41 quantifying the magnitude of the sensitivity of this C sink to its driving factors helps to
42 increase confidence in future projections of the coupled C cycle/climate system.

43 Increasing plant growth is a robust response to increasing CO₂ concentrations under
44 experimental conditions (CO₂ fertilization effect)^{7,8}. The extent to which increases in
45 CO₂ can enhance large-scale photosynthesis and ultimately net ecosystem production
46 (NEP) remains uncertain^{5,7}. Detecting this effect in the real world is much more difficult
47 than under controlled experiments. However, recent efforts using eddy-covariance-
48 based data and statistical models have been successful in detecting positive effects of
49 CO₂ on water-use efficiency (WUE)⁹, photosynthesis, and NEP⁵.

50 The potential positive effect of elevated CO₂ on productivity could be influenced by
51 global warming⁶ and altered precipitation patterns¹⁰ since both water availability and
52 temperature are strong drivers of photosynthesis and respiration worldwide^{11–13}. Land-
53 use change also alters the capacity of the biosphere to sequester C because land use
54 causes a drastic change in C turnover and productivity. Atmospheric deposition of
55 nitrogen (N) and sulphur (S) from the use of fossil fuels and fertilisers may also alter
56 ecosystem biodiversity, function, productivity and NEP^{5,14–17}. N deposition is usually
57 positively correlated with ecosystem productivity and NEP^{17–19}. Conversely, S
58 deposition may reduce ecosystem carbon sinks, this has rarely been investigated in
59 field studies^{20,21} and absent from global models. Soil acidification, caused by acid
60 deposition, of N and S, often decreases the availability of soil nutrients²² and potentially
61 reduces NEP²³.

62 The observations underlying the driver analysis of NEP described above were largely
63 limited to temperate and boreal study sites, making it difficult to assess global
64 scalability. Additionally, until recently, the only way to assess terrestrial C sink was from
65 ensembles of dynamic global vegetation models (DGVMs) or as a residual sink, by
66 subtracting atmospheric and ocean sinks to the estimates of CO₂ emissions. Currently,
67 inversion models, as well as long-term remotely sensed data²⁴, can be used to test the
68 generality of the patterns derived from ground-based measurements. Inversion models
69 provide continuous gridded estimates for the net flux of land-atmosphere CO₂
70 exchange (i.e. NEP) with global coverage^{25,26}. The gridded NEP results from
71 inversions, combined with CO₂-concentration records, gridded fields for climate, land-

72 use change, and atmospheric deposition, are arguably the best observation-based data
73 to attempt a first empirical study of the combined effects of CO₂, changes in climate
74 and land use, and atmospheric N and S deposition on terrestrial NEP patterns at the
75 global scale. Given that previous site level studies revealed that increasing CO₂ is a
76 dominant driver of trends in NEP, we expect that it will also be the dominant driver at
77 larger spatial scales and across the globe.

78 Here we investigate if the trends of NEP from the two most widely used multi-decadal
79 inversion models (MACC-II and Jena CarboScope) and DGVMs (TRENDY) from 1995
80 to 2014 are related to increasing atmospheric CO₂ and changing climate (temperature,
81 precipitation, and drought). Additionally, the effect of land-use on NEP at the global
82 scale was investigated using statistical models to assess the sensitivity of NEP to the
83 abovementioned predictors. We also analysed the effect of changing rates of
84 atmospheric deposition of oxidised and reduced N and S on NEP, combined with
85 increasing CO₂ and changing climate and land use, over Europe and the USA.

86 *CO₂ and climate effects on global NEP*

87 Global land (excluding Antarctica) mean annual NEP was 2.3 ± 0.9 , 2.3 ± 1.5 and $1.6 \pm$
88 0.5 Pg C y⁻¹ (mean $\pm 1\sigma$), respectively, for MACC-II, Jena CarboScope and the
89 TRENDY ensemble during the period 1995–2014, similar in magnitude to the recent
90 global carbon budget². Both inversions and the TRENDY ensemble showed an overall
91 positive trend in NEP from 1995 to 2014. The estimated NEP increased by (mean \pm
92 1SE) 116.9 ± 6.1 Tg C y⁻¹ for the MACC-II dataset, by 178.0 ± 8.1 Tg C y⁻¹ for the Jena
93 CarboScope dataset, and by 22.5 ± 3.1 Tg C y⁻¹ for the TRENDY ensemble (**Figure 1**).
94 This supports the increases in the global carbon budget², with a lower increase of the
95 DGVMs than those shown by the inversion models. The large differences between
96 inversion models and DGVMs may arise because of the lack of information on river
97 fluxes, inadequate parameterisations concerning land management and degradation in
98 the process models or because of potential biases in inversion models. Both inversion
99 model datasets produced similar trends for many parts of the world, an increasing NEP
100 for Siberia, Asia, Oceania, and South America, and a decreasing NEP for the southern
101 latitudes of Africa. Differences between inversions emerged for Europe and North
102 America, possibly because Jena CarboScope inversion uses a larger spatial error
103 correlation of prior fluxes than MACC-II or because of other inversion settings².
104 However, their different flux priors did not drive differences in the trends between both
105 datasets, given that priors did not change over the studied period. Jena CarboScope
106 showed largely positive trends for Europe and largely negative trends for North

107 America; MACC II showed more variation in the trends for both continents. The trends
108 identified by the TRENDY ensemble agreed with atmospheric inversions for the
109 northernmost latitudes, indicating an increase in C-sink capacity, but differed from
110 those in many other regions.

111 Our analyses on temporal contributions, using the temporal anomalies of our
112 predictors, attributed the increases in global NEP to increasing CO₂ but found a
113 consistent negative impact of temperature on NEP, which limited the positive effect of
114 increasing CO₂ (**Figure 1**). These results were consistent for both datasets and most of
115 the DGVMs of the TRENDY ensemble. The predictors used in this study explained a
116 modest proportion of the variance in NEP, in contrast to the variance explained by
117 spatial variability (i.e., the pixel), which was rather high (**Supplementary Information**
118 **(SI), Section 2**). Unknown contributions to trends in NEP, the difference between all
119 contributions and the observed trend, were very close to zero for the analyses on
120 inverse models and the TRENDY ensemble (**Figure 1**). This result suggests that trends
121 were very well captured by our analyses, indicating that the methodology was able to
122 disentangle spatial from temporal variability. The sensitivity of NEP to increasing CO₂
123 averaged 0.45 ± 0.01 , 0.61 ± 0.03 and 0.23 ± 0.01 g C m⁻² ppm⁻¹ for MACC-II, Jena
124 CarboScope and TRENDY, respectively (**Table 1**), representing sensitivities over the
125 entire terrestrial surface of 60.4 ± 1.2 , 81.4 ± 3.4 and 30.7 ± 1.2 Tg C ppm⁻¹,
126 respectively. Despite lower temporal attributions for temperature than CO₂, the
127 sensitivity of NEP to temperature was high, at -3.8 ± 1.1 , -6.4 ± 2.9 and -8.1 ± 0.9 g C
128 m⁻² y⁻¹ °C⁻¹ for the MACC-II, Jena CarboScope and TRENDY models, respectively,
129 equivalent to global sensitivities of -515.7 ± 152.4 , -859.2 ± 386.3 and -1088.0 ± 118.1
130 Tg C °C⁻¹, respectively. Trends in NEP and the effect of CO₂ and temperature on NEP
131 significantly differed in magnitude amongst the datasets used, however, they all point
132 towards the same conclusion: global NEP has increased during the study period and
133 increasing CO₂ has been the most likely driving factor despite increasing temperatures
134 constraining this positive effect. The exact magnitude of the effect of increasing CO₂
135 and temperatures on global carbon cycle remains to be established

136 *Spatial variability on CO₂ and climate change effects on NEP*

137 Our statistical models for the MACC-II and Jena CarboScope datasets indicated that
138 the positive effect of CO₂ on NEP was higher in regions with higher annual precipitation
139 and that this positive effect increased with increasing temperatures (**Figure 2, SI**
140 **Section 1.1**). In contrast, our analyses using the TRENDY ensemble did not show a
141 significant interaction between CO₂ and precipitation or with temperature, highlighting

142 the different behaviour in the DGVMs compared to inversion models. We also found a
143 significant positive interaction between mean annual temperature and CO₂ for Jena
144 CarboScope and TRENDY. However, the same interaction was negative for MACC-II.
145 On the other hand, increasing temperatures reduced NEP in warm regions but
146 increased NEP in cold regions (**Figure 2**).

147 The analyses on temporal contributions performed for inversion and TRENDY NEP
148 averaged over latitudinal bands (boreal, >55°; temperate, 35-55°; subtropical, 15-35°;
149 and tropical, 15°N-15°S), further supported previous results obtained at the global
150 scale (**Table 2, SI Sections 2.2–2.7**). Increasing CO₂ was the main factor accounting
151 for increasing trends in NEP, with a consistent positive temporal contribution for almost
152 all latitudinal bands considered and for all three datasets. However, contributions
153 estimated from the TRENDY ensemble were generally lower than those of the
154 inversion models. Proportionally, increasing CO₂ accounted for more than 90% of the
155 trends in NEP in MACC-II and Jena CarboScope datasets. For the TRENDY ensemble,
156 the estimated contribution of CO₂ to the trends in global NEP was more than 2.7 times
157 higher than the estimated trends. Increasing temperatures had a negative effect for all
158 latitudinal bands for the inversion models, but most effects were not statistically
159 significant and need to be interpreted as such. Instead, our analyses for the TRENDY
160 ensemble indicated a significant negative effect for all latitudinal bands, except for the
161 temperate southern hemisphere. Similarly, the proportional contribution of temperature
162 to the trends in NEP was less than 10% for the inversion models, but accounted for
163 almost 95% of the trends estimated using the TRENDY ensemble. These results
164 suggest that the parameterisation of temperature in the DGVMs does not accurately
165 reproduce the estimation of the inverse models.

166 Despite all regions presented, on average, positive trends, the tropical regions clearly
167 had the highest contribution, across all three datasets, to global NEP trends accounting
168 for almost half of the increase (**Table 2**). Similarly, the tropical regions had the highest
169 sensitivity to CO₂ increase, accounting for more than half of the total global sensitivity
170 (**Table 1**). A similar pattern was found for temperature, although the sign of the
171 contribution was positive for MACC-II but negative for Jena CarboScope and TRENDY.
172 The contribution of the southern hemisphere to the global trends was very modest
173 compared to the contribution of the northern hemisphere using all datasets. Our results
174 using the MACC-II dataset showed that subtropical, temperate and boreal regions of
175 the northern hemisphere accounted for 44.2% of the global trends in NEP, while only
176 9.5% was attributed to subtropical and temperate regions of the southern hemisphere.
177 Using the Jena CarboScope dataset these regions accounted for 63.3% and 6.1%,

178 respectively. Differences on the regional attributions between inversion models may
179 emerge from the different interhemispheric transport models or other inversion
180 settings². Results from the TRENDY ensemble were more extreme, because they
181 indicated a negative contribution of the subtropical and temperate regions to the global
182 trends in NEP. Differences between the global estimates (trends and contributions of
183 CO₂ and temperature) and the sum of every region were low for all datasets.
184 Contribution of other variables to the trends in NEP (precipitation, drought, land-use
185 change, and unknown variables) were on average also low for most of the latitudinal
186 bands, despite the variability amongst datasets (**Table 2**).

187 *Atmospheric deposition*

188 The MACC-II and Jena CarboScope datasets showed that NEP increased over Europe
189 and the USA by 0.45 ± 0.13 and 0.68 ± 0.16 g C m⁻² y⁻¹, respectively (**Figure S1**). Our
190 temporal contribution analyses suggested that increasing atmospheric CO₂ in both
191 datasets contributed significantly to increasing NEP. NEP sensitivity to CO₂ was more
192 than two-fold higher in the Jena CarboScope than the MACC-II dataset (**Table S1**),
193 similar to the temporal contributions, at 0.22 ± 0.06 and 0.46 ± 0.07 g C m⁻² y⁻¹ ppm⁻¹
194 for the MACC-II and Jena CarboScope models, respectively. The temporal contribution
195 of decreasing N_{ox} deposition to NEP differed between the two datasets; the
196 contribution was positive for MACC-II and negative for Jena CarboScope. Our analyses
197 consequently estimated a negative sensitivity of NEP to N_{ox} for the MACC-II dataset
198 but a positive sensitivity for the Jena CarboScope dataset. Additionally, neither MACC-
199 II, nor Jena CarboScope indicated a strong impact of land use change.

200 These statistical models indicated that, in both datasets, the positive effect of CO₂ on
201 NEP was higher in regions with higher N_{RED} deposition but lower in regions with high S
202 deposition (means for MACC-II and annual anomalies for Jena CarboScope; see **SI**
203 **section 2.8**). The results for N_{ox} deposition, however, differed between the models.
204 The positive effect of CO₂ on NEP for the MACC-II dataset was constrained by the
205 annual anomalies of N_{ox} but was higher for the Jena CarboScope dataset. We also
206 estimated an overall negative but not significant sensitivity of NEP to S deposition for
207 both inversion models.

208 *CO₂ fertilisation and global NEP*

209 The positive effect of atmospheric CO₂ on NEP must originate from a stronger positive
210 effect on photosynthesis than on the sum of all respiratory processes. Increasing
211 atmospheric CO₂ concentrations have been widely reported to increase ecosystem

212 photosynthesis, mainly by two mechanisms: i) increasing carboxylation rates and
213 decreasing photorespiration²⁷, and ii) decreasing stomatal conductance and therefore
214 increasing WUE^{9,28}, which would theoretically increase photosynthesis under water
215 limitation. An increase in GPP by either mechanism may thus account for the higher
216 NEP due to increasing atmospheric CO₂. A recent global analysis suggested that most
217 of the GPP gains from CO₂ fertilization are associated with ecosystem WUE²⁹. The
218 positive interaction between CO₂ and annual precipitation that we found may not
219 support this hypothesis (**Figure 2**), given that plants living under wet conditions are
220 usually less efficient in water use. However, plants having higher water availability may
221 benefit from increasing CO₂ more than those suffering drought because photosynthesis
222 would not be water-limited.

223 Our estimates of global NEP sensitivity to CO₂ were 0.45 ± 0.01 , 0.61 ± 0.03 and 0.23
224 ± 0.01 g C m⁻² ppm⁻¹ (globally 60.4 ± 1.2 , 81.4 ± 3.4 and 30.7 ± 3.4 Tg C ppm⁻¹) for the
225 MACC-II, Jena CarboScope and TRENDY datasets, respectively, but these estimates
226 varied amongst the latitudinal bands and were inconsistent between datasets (**Table**
227 **1**). These estimates were similar to those reported in CO₂-enrichment FACE
228 experiments³⁰, despite the fact that FACE values were calculated for a much higher
229 CO₂ range for which the effect of CO₂ may saturate³¹. However, they were much lower
230 than the 4.81 ± 0.52 g C m⁻² ppm⁻¹ reported in a study using eddy-covariance flux
231 towers for a similar period⁵. The much larger areas analysed by the inverse models
232 than the footprints covered by the eddy-covariance flux towers, and FACE
233 experiments, may explain these differences between the estimates. Flux towers are
234 usually located in relatively homogenous, undisturbed ecosystems, while each pixel in
235 the inverse model aggregates information from several ecosystems (and even biomes),
236 often including non-productive land such as bare soil or cities.

237 Our results indicated that the variability of the estimates of NEP sensitivity to CO₂
238 amongst the latitudinal bands might be associated with differences in climate and
239 atmospheric N and S deposition. The two atmospheric inversion models indicated that
240 the effect of CO₂ fertilisation was stronger in wet climates (high annual precipitation)
241 (**Figure 2**), supporting the estimates provided by the latitudinal bands, with the highest
242 sensitivity estimates for the tropical band (**Table 1**). However, analyses based on the
243 TRENDY ensemble did not show the same results. The positive effect of CO₂ tended to
244 increase with temperature anomalies in both inversion models, but, again, the DGVMs
245 did not show the same behaviour. These differences between inversion models and
246 process-based models suggest that DGVMs still fail to capture some of the interactions
247 occurring in nature. The MACC-II and Jena CarboScope datasets further agreed on a

248 stronger positive effect of increasing CO₂ in regions with higher N_{RED} deposition, which
249 confirms previous studies suggesting that the effect of CO₂ fertilisation is stronger in
250 nitrogen-rich sites^{32–34}.

251 *Climate, land-use and C sinks*

252 Climatic warming clearly had a secondary effect on the trends in NEP from 1995 to
253 2014. The MACC-II, Jena CarboScope and TRENDY datasets estimated that NEP
254 decreased globally by around -0.5 ± 0.2 , -0.9 ± 0.4 and -1.1 ± 0.1 Pg C for every
255 degree of increase in the Earth's temperature. Assuming that a CO₂ increase of 100
256 ppm is equivalent to an increase of global temperature of 1 °C, the effect of the
257 increasing CO₂ concentrations largely outweighs the negative effect of increasing
258 temperature on NEP (global estimates: 6.0 ± 0.1 , 8.1 ± 0.3 and 3.1 ± 0.1 Pg C for a
259 100 ppm of CO₂ increase according to MACC-II, Jena CarboScope and TRENDY). The
260 difference, though, is much lower for TRENDY than for the inversion models, having a
261 higher negative impact of temperature and a lower positive effect of CO₂. This
262 difference in the effects of temperature and CO₂ may explain the lower trends observed
263 in TRENDY datasets compared to MACC-II and Jena CarboScope. It also suggests
264 that a different parameterisation of temperature, CO₂ and their interaction may be
265 needed on DGVMs to capture the observed trends in the inversion models.

266 The quasi monotonically increasing atmospheric CO₂ concentrations have been more
267 important than temperature in driving NEP trends. Increasing temperature, however,
268 did not have the same effect on NEP around the world. The analyses of both inverse
269 models indicated that increasing temperatures had a positive effect on NEP only in cold
270 regions (when MAT ≤ 1.5 , 9 and -5.9 °C for MACC-II and Jena CarboScope and
271 TRENDY respectively, when CO₂ = 400 ppm, see **SI section 2.1**, and **Figure 2**).
272 These findings support previous literature reporting a positive effect between
273 temperature increase and NEP in temperate and boreal forests³⁵. Instead, the general
274 negative effect of temperature on NEP could be due to a greater stimulation of Re than
275 photosynthesis by higher temperatures^{36,37}. The potential benefit to C sequestration of
276 increased photosynthesis would then be negated by a greater increase in Re.
277 Increasing temperatures can also be linked to heat waves and drier conditions, which
278 may decrease GPP more than Re³⁸.

279 The effects of land-use change on NEP trends differed greatly amongst the datasets,
280 both at the global scale and when using latitudinal bands. Our statistical models
281 identified several significant relationships between NEP and land-use change, but the
282 large differences in effects (direction and magnitude) amongst the datasets preclude

283 drawing firm conclusions. The coarse resolution of analysis likely blurred the effects of
284 land-use change on the NEP trends.

285 Our study highlights the dominant role of rising atmospheric CO₂ concentrations
286 triggering an increase in land C sinks over the entire planet from 1995 to 2014, with the
287 tropics accounting for around half of this increase in NEP despite being only around
288 22% of the global land (excluding Antarctica, **Table 2**). Therefore, preserving tropical
289 ecosystems should be a global priority in order to mitigate anthropogenic CO₂
290 emissions. Temperature has diminished the capacity of terrestrial ecosystems to
291 sequester C, which jeopardises future C sink capacity in light of global warming. So far,
292 our results suggest that the benefit of increasing atmospheric concentrations of CO₂
293 are still compensating the negative ones of temperature rise, in terms of C
294 sequestration. However, if it has not started to change already⁶, this pattern may
295 eventually reverse with saturation of land C sinks^{5,31} or because warm ecosystems tend
296 to decrease NEP as temperature rises (**Figure 2**). Additionally, the comparison
297 between model results indicated that the DGVMs were unable to reproduce several
298 features of the global land C sinks observed in inversion models. Process-based earth
299 system models will need to improve their parameterisation to capture these features in
300 order to better predict the future of land C sinks.

301

302 **References:**

- 303 1. Canadell, J. G. *et al.* Contributions to accelerating atmospheric CO₂ growth from
304 economic activity, carbon intensity, and efficiency of natural sinks. *Proc. Natl.*
305 *Acad. Sci. U. S. A.* **104**, 18866–70 (2007).
- 306 2. Le Quéré, C. *et al.* Global Carbon Budget 2017. *Earth Syst. Sci. Data* **10**, 405–
307 448 (2018).
- 308 3. Ciais, P. *et al.* Europe-wide reduction in primary productivity caused by the heat
309 and drought in 2003. *Nature* **437**, 529–533 (2005).
- 310 4. Crowther, T. W. *et al.* Quantifying global soil carbon losses in response to
311 warming. *Nature* **540**, 104–108 (2016).
- 312 5. Fernández-Martínez, M. *et al.* Atmospheric deposition, CO₂, and change in the
313 land carbon sink. *Sci. Rep.* **7:9632**, 1–13 (2017).
- 314 6. Peñuelas, J. *et al.* Shifting from a fertilization-dominated to a warming dominated
315 period. *Nat. Ecol. Evol.* **1**, 1438–1445 (2017).
- 316 7. Ainsworth, E. A. & Long, S. P. What have we learned from 15 years of free-air
317 CO₂ enrichment (FACE)? A meta-analytic review of the responses of
318 photosynthesis, canopy properties and plant production to rising CO₂. *New*
319 *Phytol.* **165**, 351–71 (2005).
- 320 8. Medlyn, B. E. *et al.* Using ecosystem experiments to improve vegetation models.
321 *Nat. Clim. Chang.* **5**, 528–534 (2015).
- 322 9. Keenan, T. F. *et al.* Increase in forest water-use efficiency as atmospheric
323 carbon dioxide concentrations rise. *Nature* **499**, 324–327 (2013).
- 324 10. Alexander, L. *et al.* *Climate Change 2013: The Physical Science Basis -*
325 *Summary for Policymakers. Fifth Assessment Report* (Intergovernmental Panel
326 on Climate Change, 2013).
- 327 11. Fernández-Martínez, M. *et al.* Spatial variability and controls over biomass
328 stocks, carbon fluxes and resource-use efficiencies in forest ecosystems. *Trees,*
329 *Struct. Funct.* **28**, 597–611 (2014).
- 330 12. Beer, C. *et al.* Terrestrial gross carbon dioxide uptake: global distribution and
331 covariation with climate. *Science (80-.).* **329**, 834–8 (2010).

- 332 13. Luysaert, S. *et al.* CO₂ balance of boreal, temperate, and tropical forests
333 derived from a global database. *Glob. Chang. Biol.* **13**, 2509–2537 (2007).
- 334 14. de Vries, W. & Posch, M. Modelling the impact of nitrogen deposition, climate
335 change and nutrient limitations on tree carbon sequestration in Europe for the
336 period 1900–2050. *Environ. Pollut.* **159**, 2289–2299 (2011).
- 337 15. Wamelink, G. W. W. *et al.* Modelling impacts of changes in carbon dioxide
338 concentration, climate and nitrogen deposition on carbon sequestration by
339 European forests and forest soils. *For. Ecol. Manage.* **258**, 1794–1805 (2009).
- 340 16. Wamelink, G. W. W. *et al.* Effect of nitrogen deposition reduction on biodiversity
341 and carbon sequestration. *For. Ecol. Manage.* **258**, 1774–1779 (2009).
- 342 17. de Vries, W., Du, E. & Butterbach-Bahl, K. Short and long-term impacts of
343 nitrogen deposition on carbon sequestration by forest ecosystems. *Curr. Opin.*
344 *Environ. Sustain.* **9–10**, 90–104 (2014).
- 345 18. Luysaert, S. *et al.* The European carbon balance. Part 3: forests. *Glob. Chang.*
346 *Biol.* **16**, 1429–1450 (2010).
- 347 19. Magnani, F. *et al.* The human footprint in the carbon cycle of temperate and
348 boreal forests. *Nature* **447**, 848–850 (2007).
- 349 20. Thomas, R. B., Spal, S. E., Smith, K. R. & Nippert, J. B. Evidence of recovery of
350 *Juniperus virginiana* trees from sulfur pollution after the Clean Air Act. *Proc. Natl.*
351 *Acad. Sci. U. S. A.* **110**, 15319–24 (2013).
- 352 21. Oulehle, F. *et al.* Major changes in forest carbon and nitrogen cycling caused by
353 declining sulphur deposition. *Glob. Chang. Biol.* **17**, 3115–3129 (2011).
- 354 22. Truog, E. Soil Reaction Influence on Availability of Plant Nutrients¹. *Soil Sci.*
355 *Soc. Am. J.* **11**, 305 (1946).
- 356 23. Fernández-Martínez, M. *et al.* Nutrient availability as the key regulator of global
357 forest carbon balance. *Nat. Clim. Chang.* **4**, 471–476 (2014).
- 358 24. Zhu, Z. *et al.* Greening of the Earth and its drivers. *Nat. Clim. Chang.* **6**, 791–795
359 (2016).
- 360 25. Chevallier, F. *et al.* CO₂ surface fluxes at grid point scale estimated from a
361 global 21 year reanalysis of atmospheric measurements. *J. Geophys. Res.* **115**,

- 362 D21307 (2010).
- 363 26. Rödenbeck, C., Houweling, S., Gloor, M. & Heimann, M. CO₂ flux history 1982–
364 2001 inferred from atmospheric data using a global inversion of atmospheric
365 transport. *Atmos. Chem. Phys.* **3**, 1919–1964 (2003).
- 366 27. Aber, J. *et al.* Forest Processes and Global Environmental Change: Predicting
367 the Effects of Individual and Multiple Stressors. *Bioscience* **51**, 735 (2001).
- 368 28. Prentice, I. C., Heimann, M. & Sitch, S. The carbon balance of the terrestrial
369 biosphere: Ecosystem models and Atmospheric observations. *Ecol. Appl.* **10**,
370 1553–1573 (2000).
- 371 29. Cheng, L. *et al.* Recent increases in terrestrial carbon uptake at little cost to the
372 water cycle. *Nat. Commun.* **8**, 110 (2017).
- 373 30. Norby, R. J., Warren, J. M., Iversen, C. M., Medlyn, B. E. & McMurtrie, R. E.
374 CO₂ enhancement of forest productivity constrained by limited nitrogen
375 availability. *Proc. Natl. Acad. Sci. U. S. A.* **107**, 19368–73 (2010).
- 376 31. Norby, R. J. *et al.* Forest response to elevated CO₂ is conserved across a broad
377 range of productivity. *Proc. Natl. Acad. Sci. U. S. A.* **102**, 18052–18056 (2005).
- 378 32. Van Groenigen, K. J. *et al.* The Impact of Elevated Atmospheric CO₂ on Soil C
379 and N Dynamics. *Ecol. Stud.* **187**, 374–391 (2006).
- 380 33. Terrer, C. *et al.* Mycorrhizal association as a primary control of the CO₂
381 fertilization effect. *Science* **353**, 72–4 (2016).
- 382 34. McCarthy, H. R. *et al.* Re-assessment of plant carbon dynamics at the Duke
383 free-air CO₂ enrichment site: interactions of atmospheric [CO₂] with nitrogen and
384 water availability over stand development. *New Phytol.* **185**, 514–528 (2010).
- 385 35. Hyvönen, R. *et al.* The likely impact of elevated [CO₂], nitrogen deposition,
386 increased temperature and management on carbon sequestration in temperate
387 and boreal forest ecosystems: a literature review. *New Phytol.* **173**, 463–80
388 (2007).
- 389 36. Ryan, M. G. Effects of climate change on plant respiration. *Ecol. Appl.* **1**, 157–
390 167 (1991).
- 391 37. Amthor, J. S. Scaling CO₂ Photosynthesis Relationships from the Leaf to the

- 392 Canopy. *Photosynth. Res.* **39**, 321–350 (1994).
- 393 38. Wu, Z., Dijkstra, P., Koch, G. W., Peñuelas, J. & Hungate, B. a. Responses of
394 terrestrial ecosystems to temperature and precipitation change: a meta-analysis
395 of experimental manipulation. *Glob. Chang. Biol.* **17**, 927–942 (2011).
- 396 39. Chevallier, F. *et al.* Toward robust and consistent regional CO₂ flux estimates
397 from in situ and spaceborne measurements of atmospheric CO₂. *Geophys. Res.*
398 *Lett.* **41**, 1065–1070 (2014).
- 399 40. Olivier, J. G. J. & Berdowski, J. J. M. in *The Climate System* (eds. Berdowski, J.,
400 Guicherit, R. & Heij, B. J.) 33–78 (2001).
- 401 41. Sitch, S. *et al.* Recent trends and drivers of regional sources and sinks of carbon
402 dioxide. *Biogeosciences* **12**, 653–679 (2015).
- 403 42. Harris, I., Jones, P. D. D., Osborn, T. J. J. & Lister, D. H. H. Updated high-
404 resolution grids of monthly climatic observations - the CRU TS3.10 Dataset. *Int.*
405 *J. Climatol.* **34**, online, update (2013).
- 406 43. Vicente-serrano, S. M., Beguería, S. & López-Moreno, J. I. A Multiscalar Drought
407 Index Sensitive to Global Warming: The Standardized Precipitation
408 Evapotranspiration Index. *J. Clim.* **23**, 1696–1718 (2010).
- 409 44. Zuur, A., Ieno, E., Walker, N., Saveliev, A. & Smith, G. *Mixed effects models and*
410 *extensions in ecology with R*. (Springer science, 2009).
- 411 45. Mathias, J. M. & Thomas, R. B. Disentangling the effects of acidic air pollution,
412 atmospheric CO₂, and climate change on recent growth of red spruce trees in
413 the Central Appalachian Mountains. *Glob. Chang. Biol.* **24**, 3938–3953 (2018).
- 414 46. R Core Team. R: A Language and Environment for Statistical Computing. (2016).
- 415 47. Barton, K. MuMIn: Multi-model inference. R package version 1.17.1.
416 <http://CRAN.R-project.org/package=MuMIn>. (2015).
- 417 48. Nakagawa, S. & Schielzeth, H. A general and simple method for obtaining R²
418 from generalized linear mixed-effects models. *Methods Ecol. Evol.* **4**, 133–142
419 (2013).
- 420 49. Breheny, P. & Burchett, W. Visualization of Regression Models Using visreg, R
421 package version 2.2-0. (2015).

422 **Correspondence and requests for materials should be addressed to:**

423 Marcos Fernández-Martínez: marcos.fernandez-martinez@uantwerpen.be

424 **Acknowledgements**

425 This research was supported by the Spanish Government project CGL2016-79835-P
426 (FERTWARM), the European Research Council Synergy grant ERC-2013-726 SyG-
427 610028 IMBALANCE-P, and the Catalan Government project SGR 2017-1005. M.F-M
428 and S.V. are a postdoctoral fellows of the Research Foundation – Flanders (FWO).
429 J.G.C. thanks the support of the National Environmental Science Programme ESCC
430 Hub. We thank Christian Röedenbeck for his advice and for distributing Jena
431 CarboScope and all the modellers that contributed to the TRENDY project.

432

433 **Author Contributions**

434 M.F-M., J.S., I.A.J., and J.P. conceived, analyzed and wrote the paper. F.C., P.F., and
435 S.S., provided data. All authors contributed substantially to the writing and discussion
436 of the paper.

437

438 **Figure captions**

439 **Figure 1: Global trends in NEP and their contributing factors.** Global temporal
440 contributions of CO₂, climate and land-use change to the trends in NEP (annual
441 change) are shown on the right side of each panel. The difference between the
442 modelled temporal contributions and the trends (shaded) has been treated as an
443 unknown contribution to the temporal variation in NEP. Statistically significant ($P <$
444 0.01) temporal variations of the predictors are shown in square brackets. Error bars
445 indicate 95% confidence intervals. The boxplots in panel c indicate the estimated
446 contributions of the 10 DVGMs used in the TRENDY ensemble. Units are ppm y⁻¹ for
447 CO₂, °C y⁻¹ for temperature, mm y⁻² for precipitation, standard deviation for SPEI, and
448 percentage of land-use cover per pixel for forests, crops, and urban areas. See the
449 Materials and Methods section for information about the methodology used to calculate
450 the contributions. Significance levels: *, $P < 0.01$; **, $P < 0.005$; ***, $P < 0.001$.

451 **Figure 2: Plots showing the estimated effects of the interactions of the statistical**
452 **models.** The graphs show interactions between CO₂ and climate (mean annual
453 precipitation [MAP] and temperature [MAT], and annual anomalies in temperature
454 [MAT.an]) on NEP for the MACC-II and Jena CarboScope inversion models and the
455 TRENDY ensemble. Shaded bands indicate the 95% confidence intervals of the
456 slopes. Non-significant interactions are indicated by “n.s.”.

457 **Table 1: Global and latitudinal analyses of sensitivity of NEP to changes in**
458 **atmospheric CO₂ concentrations and mean annual temperature.** The “%” columns
459 indicate the contribution of the latitudinal band to the global estimate. Differences are
460 calculated as the difference between the sum of all latitudinal bands and the global
461 estimate. Bold coefficients differ significantly from 0 at the 0.01 level. Empty cells
462 indicate that anomalies in temperature were not a significant predictor in the models
463 predicting NEP. Units are Tg C y⁻¹ ppm⁻¹ for CO₂ and Tg C y⁻¹ C⁻¹ for temperature.

464 **Table 2: Global and latitudinal trends and temporal contributions of changes in**
465 **atmospheric CO₂ concentrations and mean annual temperature to NEP trends.**
466 The “%” columns indicate the percentage of contribution of each latitudinal band to the
467 global estimate. Columns “Cont.” show the percentage of contribution of CO₂ and
468 temperature to the trends in NEP. Column “Other” shows the difference between the
469 NEP trend and the sum of contributions of CO₂ and temperature. If different from zero,
470 it indicates that other factors are contributing to the trends in NEP. The “differences”
471 rows are calculated as the difference between the sum of all latitudinal bands and the

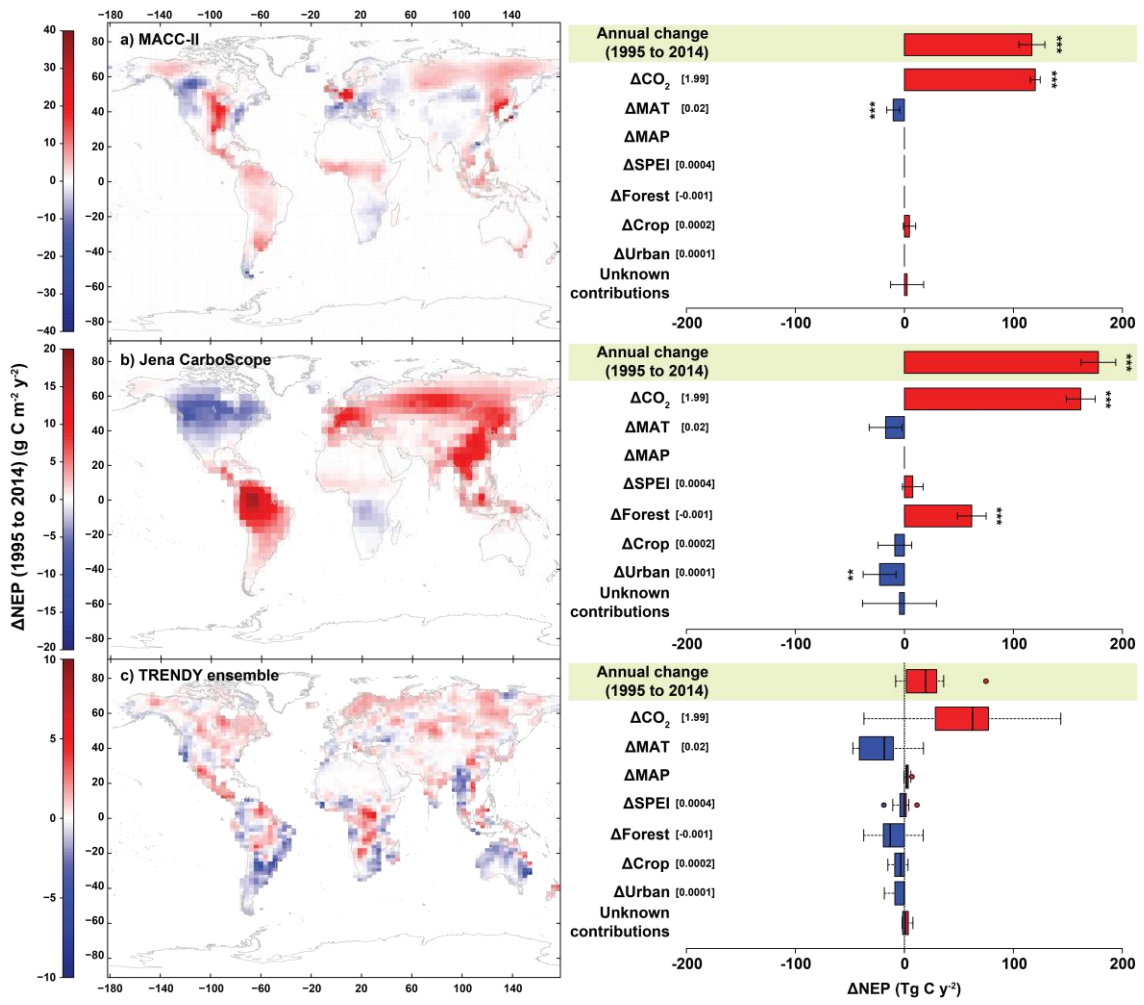
472 global estimate. NH and SH indicate Northern and Southern Hemispheres,
473 respectively. Bold coefficients differ significantly from 0 at the 0.01 level. Empty cells
474 indicate that anomalies in temperature were not a significant predictor in the models
475 predicting NEP. Units are Tg C y⁻¹ for trends, Tg C y⁻¹ ppm⁻¹ for CO₂ and Tg C y⁻¹ C⁻¹
476 for temperature. Errors were calculated using the error propagation method. See the
477 Materials and Methods section for information about the methods used to calculate the
478 contributions.

479

480

481

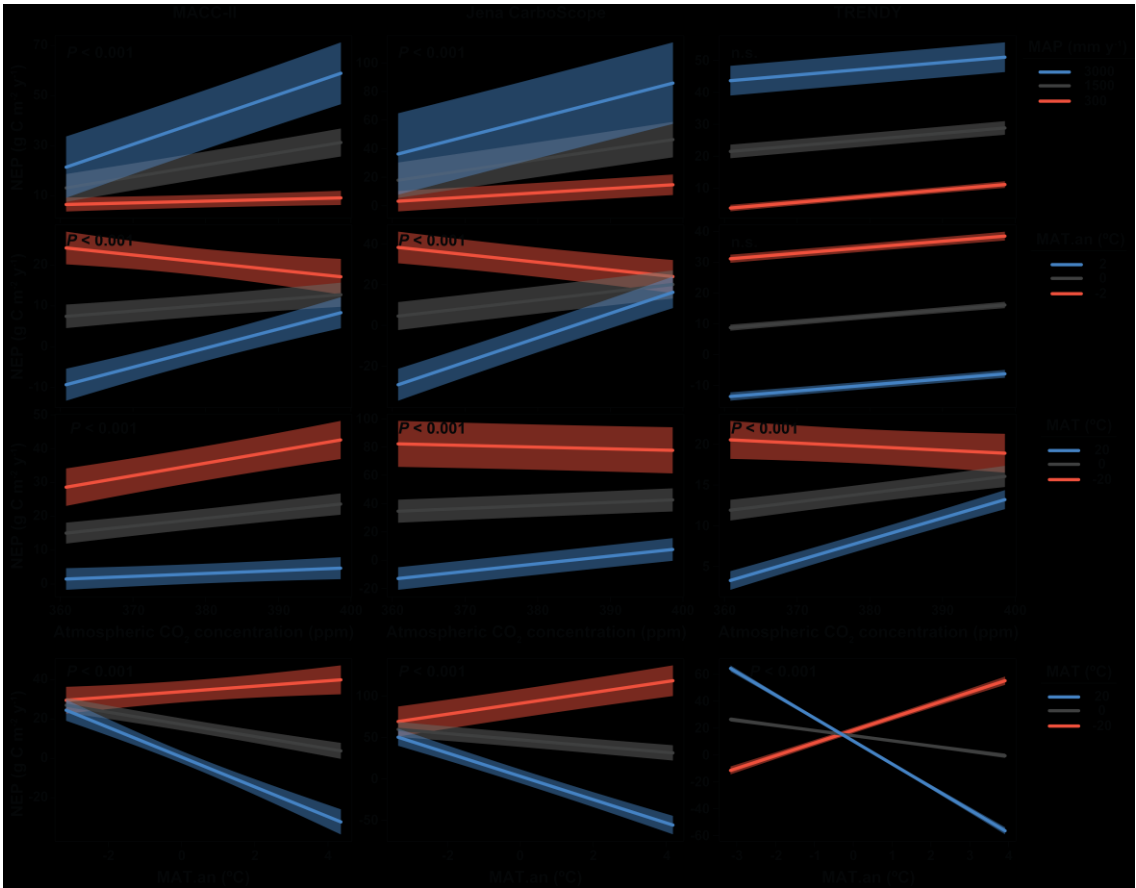
482 **Figure 1**



483

484

485 **Figure 2**



486

487

488 **Table 1**

	CO ₂	%	Temperature	%
<i>MACC</i>				
NH >55°	8.5 ± 0.4	14.1	-35.3 ± 24.1	6.8
NH 35-55°	14.7 ± 1.3	24.3	-132.0 ± 259.9	25.6
NH 15-35°	-5.0 ± 1.4	-8.3		
NH 15-SH 15°	31.9 ± 0.7	52.9	101.9 ± 216.6	-19.8
SH 15-35°	2.2 ± 0.9	3.7	-150.2 ± 131.3	29.1
SH 35-55°	0.6 ± 0.3	1.0	-13.4 ± 49.3	2.6
Global	60.4 ± 1.2		-515.7 ± 152.4	
Difference	-7.4 ± 2.6	-12.3	286.6 ± 397.4	-55.6
<i>JENA</i>				
NH >55°	-0.3 ± 1.0	-0.3	-49.8 ± 48.2	5.8
NH 35-55°	11.1 ± 3.9	13.6	-213.6 ± 558.1	24.9
NH 15-35°	26.3 ± 2.7	32.3	-268.7 ± 400.0	31.3
NH 15-SH 15°	54.2 ± 3.6	66.6	-697.6 ± 1136.5	81.2
SH 15-35°	5.4 ± 0.9	6.6	-167.0 ± 133.9	19.4
SH 35-55°	0.2 ± 0.0	0.3		
Global	81.4 ± 3.4		-859.2 ± 386.3	
Difference	15.4 ± 6.9	19.0	-537.4 ± 1390.2	62.5
<i>TRENDY</i>				
NH >55°	2.8 ± 0.1	9.0	17.3 ± 7.3	-1.6
NH 35-55°	5.8 ± 0.5	19.0	-251.1 ± 79.3	23.1
NH 15-35°	5.9 ± 0.6	19.4	-368.8 ± 51.9	33.9
NH 15-SH 15°	16.6 ± 1.1	54.2	-1612.2 ± 213.4	148.2
SH 15-35°	4.6 ± 1.2	14.9	-379.2 ± 141.1	34.9
SH 35-55°	0.3 ± 0.2	1.0	-36.8 ± 18.1	3.4
Global	30.7 ± 1.2		-1088.0 ± 118.1	
Difference	5.4 ± 2.1	17.5	-1542.7 ± 298.0	141.8

490 **Table 2**

	Trends	%	CO ₂	%	Cont.	Temp	%	Cont.	Other
<i>MACC</i>									
NH >55°	20.1 ± 1.2	17.2	17.0 ± 0.8	14.1	84.4	-1.2 ± 0.8	11.5	-5.9	4.3 ± 1.7
NH 35-55°	17.5 ± 5.0	15.0	29.2 ± 2.7	24.3	166.6	-1.7 ± 3.2	16.1	-9.4	-10.0 ± 6.5
NH 15-35°	14.0 ± 3.1	12.0	-9.9 ± 2.8	-8.3	-71.0			0.0	23.9 ± 4.1
NH 15- SH 15°	55.4 ± 2.7	47.4	63.5 ± 1.5	52.9	114.6	0.9 ± 1.9	-8.9	1.6	-9.0 ± 3.6
SH 15-35°	7.6 ± 1.4	6.5	4.4 ± 1.9	3.7	57.6	-2.3 ± 2.0	22.2	-29.8	5.5 ± 3.1
SH 35-55°	2.3 ± 0.6	2.0	1.2 ± 0.7	1.0	49.9	-0.3 ± 1.0	2.5	-11.2	1.4 ± 1.3
Global	116.9 ± 6.1		120.1 ± 2.3		102.7	-10.3 ± 3.0		-8.8	7.1 ± 7.2
Difference	0.0 ± 9.1	0.0	-14.8 ± 5.2	-12.3		5.8 ± 5.4	-56.6		
<i>JENA</i>									
NH >55°	13.8 ± 2.2	7.7	-0.5 ± 2.1	-0.3	-3.8	-1.7 ± 1.7	9.9	-12.4	16.0 ± 3.5
NH 35-55°	49.8 ± 5.9	28.0	22.0 ± 7.7	13.6	44.1	-2.7 ± 6.9	15.4	-5.3	30.5 ± 11.9
NH 15-35°	49.2 ± 4.0	27.6	52.3 ± 5.3	32.3	106.2	-5.0 ± 7.4	29.0	-10.2	1.9 ± 10.0
NH 15- SH 15°	80.4 ± 5.1	45.2	107.7 ± 7.1	66.6	133.9	-5.7 ± 9.2	32.9	-7.0	-21.6 ± 12.7
SH 15-35°	10.4 ± 1.3	5.8	10.7 ± 1.7	6.6	103.1	-2.8 ± 2.2	16.2	-26.9	2.5 ± 3.1
SH 35-55°	0.5 ± 0.1	0.3	0.4 ± 0.1	0.3	87.2				0.1 ± 0.1
Global	178.0 ± 8.1		161.8 ± 6.8		90.9	-17.2 ± 7.7		-9.7	33.4 ± 13.1
Difference	26.1 ± 12.2	14.7	30.7 ± 13.8	19.0		-0.6 ± 16.0	3.4		
<i>TRENDY</i>									
NH >55°	9.3 ± 0.6	41.4	5.5 ± 0.3	9.0	59.0	0.6 ± 0.2	-2.7	6.1	3.3 ± 0.7
NH 35-55°	9.4 ± 1.3	41.5	11.6 ± 0.9	19.0	124.0	-3.0 ± 0.9	13.9	-31.6	0.7 ± 1.8
NH 15-35°	3.3 ± 1.3	14.9	11.8 ± 1.1	19.4	352.9	-7.9 ± 1.0	36.9	-235.0	-0.6 ± 2.0
NH 15- SH 15°	10.1 ± 2.3	45.0	33.0 ± 2.1	54.2	326.2	-17.2 ± 1.8	80.8	-170.2	-5.7 ± 3.6
SH 15-35°	-13.7 ± 1.8	-60.9	0.5 ± 0.1	0.9	-3.8	-0.3 ± 0.1	1.6	2.5	-13.9 ± 1.8
SH 35-55°	-1.0 ± 0.4	-4.7	0.6 ± 0.5	1.0	-55.4	-0.7 ± 0.4	3.5	70.4	-0.9 ± 0.7
Global	22.5 ± 3.1		61.0 ± 2.5		270.7	-21.3 ± 2.2		-94.7	-17.1 ± 4.5
Difference	-5.2 ± 4.7	-22.9	2.1 ± 3.6	3.4		-7.3 ± 3.2	34.0		

491

492

493 **Methods**

494 Datasets

495 *NEP data*

496 We used gridded global monthly NEP data for 1995–2014 from two inversion models: i)
497 the MACC (Monitoring Atmospheric Composition and Climate) CO₂ ([http://www.gmes-
498 atmosphere.eu/catalogue/](http://www.gmes-atmosphere.eu/catalogue/))^{25,39} database, version v14r2 and ii) the Jena CarboScope
499 database version s93_v3.7 using a constant network of towers ([http://www.bgc-
500 jena.mpg.de/CarboScope/](http://www.bgc-jena.mpg.de/CarboScope/))²⁶. The MACC CO₂ atmospheric inversion system relies on
501 the variational formulation of Bayes' theorem to analyse direct measurements of CO₂
502 concentrations from 130 sites around the globe for 1979-2014. Optimised fluxes were
503 calculated at a global horizontal resolution of 3.75 × 1.875° (longitude, latitude) and a
504 temporal resolution of eight days, separately for daytime and night-time. The underlying
505 transport model was run with interannually varying meteorological data from the
506 ECMWF ERA-Interim reanalysis. The Jena inversion model estimates the interannual
507 variability of CO₂ fluxes based on raw CO₂ concentration data from 50 sites. The model
508 uses a variational approach with the TM3 transport model (4 × 5°, using interannually
509 varying winds). Prior terrestrial fluxes were obtained from a modelled mean biospheric
510 pattern and fossil-fuel emissions from the EDGAR emission database⁴⁰. We also used
511 NEP data from an ensemble of 10 dynamic global vegetation models (DGVMs)
512 compiled by the TRENDY project (version 4, models CLM4.5, ISAM, JSBACH, JULES,
513 LPJG, LPX, OCN, ORCHIDEE, VEGAS, and VISIT) to see if results obtained from
514 atmospheric inversions data match those obtained with DGVMs simulations⁴¹. We used
515 the output from simulation experiment S3, which was run with varying atmospheric CO₂
516 and changing land use and climate⁴¹.

517 *Meteorological, land-use change and atmospheric CO₂ data*

518 We extracted gridded temperature and precipitation time series from the Climatic
519 Research Unit TS3.23 dataset⁴². We also used the SPEI (Standardised Precipitation-
520 Evapotranspiration Index) drought index⁴³ from the global SPEI database
521 (<http://SPEI.csic.es/database.html>) as a measure of drought intensity (positive values
522 indicate wetter than average meteorological conditions, negative values indicate drier
523 than average conditions). We used annual SPEI1 (monthly SPEI averaged over a
524 year). Mean annual temperature (MAT) and precipitation (MAP) and SPEI were
525 calculated for each year and pixel. We used land-use change maps from land-use
526 harmonisation² (LUH2, <http://luh.umd.edu/data.shtml>) and calculated the percent

527 coverages of forests, croplands, and urban areas per pixel, so we could further
528 estimate whether they increased or decreased from 1995 to 2014. We used the data
529 for atmospheric CO₂ concentration from Mauna Loa Observatory provided by the
530 Scripps Institution of Oceanography (Scripps CO₂ programme).

531 *Data for N and S deposition*

532 Annual data for N (oxidised N [N_{OX}] from NO₃⁻ and reduced N [N_{RED}] from NH₄⁺) and S
533 (SO₄⁻) wet deposition were extracted from: i) the European Monitoring and Evaluation
534 Programme (EMEP) with a spatial resolution of 0.15 × 0.15° for longitude and latitude,
535 ii) the MSC-W chemical-transport model developed to estimate regional atmospheric
536 dispersion and deposition of acidifying and eutrophying N and S compounds over
537 Europe, and iii) the National Atmospheric Deposition Program (NADP) covering the
538 USA with a spatial resolution of 0.027 × 0.027° for longitude and latitude. We used only
539 data for wet deposition because the NADP database only contained records for dry
540 deposition for 2000. Analyses focused on atmospheric deposition and were restricted
541 to Europe and the USA because temporal gridded maps of atmospheric deposition
542 were not available for other regions. Maps of atmospheric deposition for the regional
543 analyses were adjusted to the resolution of the C-flux maps (3.75 × 1.875° for the
544 MACC-II model and 4 × 5° for the Jena CarboScope model for longitude and latitude).

545 Statistical analyses

546 *Gridded, global and regional trend detection on NEP*

547 To determine how NEP has changed from 1995 to 2014, we first calculated the trends
548 for each pixel in both inversion models and an average dataset of the TRENDY
549 ensemble using linear regressions with an autoregressive and moving-average
550 (ARMA) (autoregressive structure at lag p=1, and no moving average q=0) correlation
551 structure to account for temporal autocorrelation. Trends over larger areas (e.g. the
552 entire world, latitudinal bands), either for NEP or the predictor variables, were
553 calculated using generalised linear mixed models (GLMMs) with random slopes,
554 including also random intercepts⁴⁴ (e.g. NEP ~ year). We used pixel as the random
555 factor (affecting the intercepts and slopes of the year), and an ARMA (p=1, q=0)
556 correlation structure. All average trends shown were calculated using this methodology.

557 *Calculation of temporal contributions on trends of NEP*

558 The temporal contributions of increasing CO₂, climate (MAT, MAP, and SPEI), and
559 land-use change (forests, croplands, and urban areas) to the observed trends in NEP

560 were assessed for the MACC-II, Jena CarboScope, and TRENDY datasets for the
561 entire world. We repeated the analysis for five latitudinal bands to determine if the
562 contributions of CO₂, climate, and land-use change were globally consistent using
563 MACC-II, Jena CarboScope, and the mean ensemble of the TRENDY datasets. For the
564 MACC-II and Jena CarboScope datasets, we also determined the temporal contribution
565 of atmospheric deposition of N (N_{OX} and N_{RED}) and S to the trends in NEP in a
566 combined analysis that also included CO₂, climatic, and land-use trends. This latter
567 analysis was restricted to Europe and the USA due to the lack of atmospheric-
568 deposition time series for the rest of the world.

569 The temporal contributions of the predictor variables were calculated following the
570 methodology established in references^{5,45}, as follows:

571 i) using a GLMM with an autocorrelation structure for lag 1 (AR1) and using the pixel as
572 the random factor affecting only the intercept, we fitted full models for NEP as a
573 function of CO₂, mean MAT per pixel, annual anomaly of MAT, mean MAP per pixel,
574 annual anomaly of MAP, the annual SPEI, and mean percentage of forested, cropped,
575 and urban areas per pixel and their annual anomalies. We included the first-order
576 interaction terms between CO₂ and all predictors and between the mean values and
577 the anomalies for all predictors (except SPEI, which interacted with mean MAT and
578 MAP). When the interaction term between the means and the anomalies (e.g. MAT
579 mean × MAT anomaly) was included, the model estimated the effect of the anomaly as
580 a function of the average value. This implies a change in the effect of increasing or
581 decreasing the anomalies, depending on the mean for the site (e.g. increasing
582 temperature may have a positive effect in cold climates but a negative effect in warmer
583 climates). For models including atmospheric deposition, we also included the
584 interaction between climatic variables and CO₂ and the interactions between the means
585 and the annual anomalies of atmospheric deposition (N_{OX}, N_{RED}, and S). The models
586 were fitted using maximum likelihood to allow the comparison of models with different
587 fixed factors.

588 ii) We used the stepwise backwards-forwards model selection (*stepAIC* function in R⁴⁶)
589 from the full models, using the lowest Bayesian information criterion (BIC), to obtain the
590 best model. The amount of the variance explained by the models was assessed using
591 the *r.squaredGLMM* function in R (MuMIn package: ⁴⁷) following the method of
592 Nakagawa and Schielzeth (2013). Model residuals met the assumptions required in all
593 analyses (normality and homoscedasticity of residuals).

594 iii) We then used the selected models to predict the changes of the response variables
595 during the study period (1995–2014). We first extracted the observed trend (mean \pm
596 SEM, standard error of the mean) in NEP using raw data with GLMMs with an AR1
597 autocorrelation structure. We then calculated the trend of NEP predicted by the final
598 model and the trends of NEP predicted by the same model while maintaining the
599 temporally varying predictors (i.e., anomalies) constant one at a time (e.g. MAT
600 anomalies were held constant using the median per pixel, while all other predictors
601 changed based on the observations). The difference between the predictions for the
602 final model and when one predictor was controlled was assumed to be the contribution
603 of that predictor variable to the change in NEP. The differences between all individual
604 contributions and the observed trend in NEP were treated as unknown contributions.

605 *Calculation of sensitivities of NEP to temporal predictors*

606 Finally, we calculated the average sensitivities of NEP to the predictor changes by
607 dividing the temporal contributions of each predictor of delta NEP by their temporal
608 trends. Spatial variability on the effects of temporal predictors to NEP were assessed
609 using the GLMMs fitted to estimate the temporal contributions of the predictors. To
610 visualise the interactions we used the R package visreg⁴⁹. All errors were calculated
611 using the error-propagation method using the following two equations, for additions and
612 subtractions: $\epsilon C = \sqrt{(\epsilon A)^2 + (\epsilon B)^2}$; and for multiplications and divisions: $\epsilon C =$
613 $C \sqrt{\left(\frac{\epsilon A}{A}\right)^2 + \left(\frac{\epsilon B}{B}\right)^2}$; where ϵ indicates the error associated to each value (A, B or C). To
614 calculate global and regional estimates we multiplied the model outputs, in units of gC
615 m⁻², times land area. We considered the land Earth surface area to be 134375000 km²
616 excluding the Antarctic region. Land area for the different latitudinal bands used were:
617 >55° N, 23818000 km²; 35 to 55° N, 31765000 km²; 15 to 35° N, 29213000 km²; 15° S
618 to 15° N, 29926000 km²; 15 to 35° S, 17308000 km²; and 35 to 55° S, 2345600 km².

619

620 **Data availability**

621 The authors declare that the data supporting the findings of this study are publically
622 available in the webpages provided in the article. The TRENDY simulations are
623 available from the corresponding author upon request.

624